Heralded Distribution of Single-Photon Path Entanglement

P. Caspar,[1] E. Verbanis,[1] E. Oudot,[1,2] N. Maring,[1] F. Samara,[1] M. Caloz,[1] M. Perrenoud,[1] P. Sekatski,[2] A. Martin,[1,*] N. Sangouard,[2,3] H. Zbinden,[1] and R. T. Thew[1,†]
[1]*Department of Applied Physics, University of Geneva, CH-1211 Genève, Switzerland*
[2]*Quantum Optics Theory Group, University of Basel, CH-4056 Basel, Switzerland*
[3]*Institut de physique théorique, Université Paris Saclay, CEA, CNRS, F-91191 Gif-sur-Yvette, France*

(Received 24 April 2020; accepted 30 July 2020; published 10 September 2020)

We report the experimental realization of heralded distribution of single-photon path entanglement at telecommunication wavelengths in a repeater-like architecture. The entanglement is established upon detection of a single photon, originating from one of two spontaneous parametric down-conversion photon pair sources, after erasing the photon's which-path information. In order to certify the entanglement, we use an entanglement witness which does not rely on postselection. We herald entanglement between two locations, separated by a total distance of 2 km of optical fiber, at a rate of 1.6 kHz. This work paves the way towards high-rate and practical quantum repeater architectures.

DOI: 10.1103/PhysRevLett.125.110506

Sharing photonic entanglement over long distances is a key resource for building a quantum communication network [1,2]. In order to distribute entanglement to two remote parties through optical fiber, quantum repeater schemes provide a solution to overcome the direct transmission loss [3]. The basic idea is to divide the whole distance into elementary links in each of which entanglement is independently established in a heralded way between two quantum memories. Finally, successive entanglement swapping operations between the links are used to extend the entanglement over the whole distance. Among the different quantum repeater schemes, those using single-photon path entanglement [4], where a single photon is delocalized into two modes, are promising candidates for establishing such a network since they require fewer resources as well as being less sensitive to memory and detector inefficiencies compared to other repeater schemes due to their linear, rather than quadratic, loss scaling [5].

A proposed postselection-free approach for entanglement distribution, based on the erasure of the heralding photon's which-path information, is a modification of the Duan-Lukin-Cirac-Zoller (DLCZ) protocol [6] that employs photon pair sources and multimode memories [7]. A practical implementation of this scheme, however, faces two major challenges. It requires first, stabilization and control of the optical phase between the two parties, and second, a practical implementation for entanglement certification. Experiments overcoming both challenges by employing individual matter qubits have been presented with ions [8], quantum dots [9,10], and nitrogen-vacancy centers [11]. However, in all those table-top demonstrations, entanglement was heralded by a photon outside the telecom band and thus will need to be frequency converted, which will further complicate the management of phase in the network. An approach combining an atomic ensemble quantum memory at near-infrared wavelengths and quantum frequency conversion to the telecom O-band has recently been reported [12], however, the entanglement was certified by recombining the entangled modes (single-photon interference) which is not applicable in a distributed scenario.

In this work we demonstrate a scheme for the heralded distribution of single-photon path entanglement at telecom wavelengths over a distance of 2×1.0 km of optical fiber, in a quantum repeater-like architecture (see Fig. 1). The detection of a single photon at the central station erases the which-path information about which one of the two photon pair sources it was emitted from, and heralds the distributed entangled state. The fiber connecting Alice and Bob is part of a phase stabilized interferometer. Another fiber (not shown), between Alice and Bob, closes the interferometer and is connected to a laser that is used to stabilize the interferometer. Inspired by an entanglement witness [13] using displacement-based photon detections [14], the

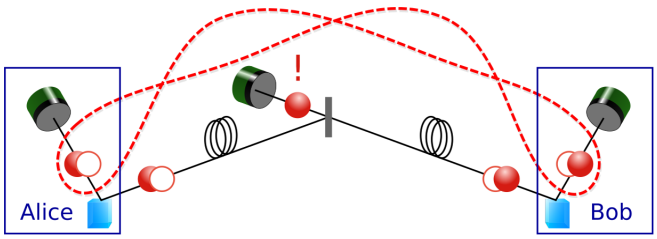

FIG. 1. Conceptual schematic of the experiment. A successful detection of a photon at the central station, originating from one of two photon pair sources, heralds the distribution of a single-photon path-entangled state between Alice and Bob.

 © 2020 American Physical Society

distributed entanglement is measured locally and certified by an entanglement witness that is robust to loss, and does not make assumptions about the state itself.

Concept.—Each of the two spontaneous parametric down conversion (SPDC) photon pair sources, held by Alice and Bob, creates a two-mode squeezed vacuum state with low photon pair creation probability per pump pulse $P_{\mathrm{pair},A} = P_{\mathrm{pair},B} \ll 1$. Two modes, one from each source, are combined on a 50/50 beam splitter at the central station. By neglecting contributions from higher order pair creation probabilities $\mathcal{O}(P_{\mathrm{pair}})$, the resulting state shared between Alice and Bob, conditioned on the detection of a heralding photon, can be written as

$$|\psi\rangle_{AB} = \frac{1}{\sqrt{2}}(|10\rangle_{AB} + e^{i(\theta_B-\theta_A)}|01\rangle_{AB}), \tag{1}$$

where $|0\rangle$ denotes the vacuum state, $|1\rangle$ the single-photon number state, $\theta_{A(B)} = \phi_{A(B)} + \chi_{A(B)}$ with $\phi_{A(B)}$ the phase of the pump before the source on Alice's (Bob's) side and $\chi_{A(B)}$ the respective phase acquired by the photon traveling from the source to the central station [see Ref. [7] for the derivation of Eq. (1) and a more complete discussion]. The first conceptual challenge of this scheme is to prove entanglement within the $\{|0\rangle, |1\rangle\}$ subspace. This is possible using photon detection techniques preceded by weak displacement operations [14–19], as described in the following.

Displacement-based measurement.—We introduce the bosonic annihilation and creation operators a_i and $a_i^\dagger$ with $i \in \{1, 2\}$ acting on the photonic modes on Alice's ($i = 1$) and Bob's ($i = 2$) sides. We assume non-photon-number-resolving detectors, that is, only two different measurement results can be produced in each run. A "no-click" event is modeled by a projection on the vacuum state $|0\rangle\langle 0|$ whereas a "click" event corresponds to the projection into the orthogonal subspace $\mathbb{1} - |0\rangle\langle 0|$. If we attribute the outcome $+1$ to a no-detection and -1 to a conclusive detection, the observable including the displacement operation $D(\alpha_i) = e^{\alpha_i a_i^\dagger - \alpha_i^* a_i}$ on mode i is given by

$$\sigma_{\alpha_i}^{(i)} = D^\dagger(\alpha_i)(2|0\rangle\langle 0| - \mathbb{1})D(\alpha_i). \tag{2}$$

In the qubit subspace $\{|0\rangle, |1\rangle\}$, $\sigma_0^{(i)}$ corresponds exactly to the Pauli matrix σ_z on mode i. When α increases in amplitude, the positive operator valued measure (POVM) elements associated with outcomes $+1$ get closer to projections in the $x-y$ plane of the Bloch sphere [14]. For $\alpha = 1$ ($\alpha = i$), these POVM elements are projections along non-unit vectors pointing in the $x(y)$ direction.

Entanglement certification.—Building upon the displacement-based measurement, we now elaborate on the theory behind the witness that we developed to optimally certify path entanglement even in a lossy environment. The certification of entanglement for the state $|\psi\rangle_{AB}$ requires access to the coherence terms $|01\rangle\langle 10|$ and $|10\rangle\langle 01|$ as well as to the probabilities P_{ij} to have i photons on the first mode and j photons on the second mode. A good entanglement witness for our state is the observable

$$\hat{\mathcal{W}} = \sigma_{\alpha_1}^{(1)} \otimes \sigma_{\alpha_2}^{(2)}, \tag{3}$$

which is phase averaged according to

$$\hat{W} = \frac{1}{2\pi}\int_0^{2\pi} d\phi \left(\prod_{i=1}^{2} e^{i\phi \hat{a}_i^\dagger \hat{a}_i}\right) \hat{\mathcal{W}} \left(\prod_{i=1}^{2} e^{-i\phi \hat{a}_i^\dagger \hat{a}_i}\right) \tag{4}$$

to take into account that from experimental run to run, the global phase of the displacement parameter is arbitrary. Thus, the only remaining coherence terms in $\hat{W}$ are exactly the desired ones between $|01\rangle$ and $|10\rangle$.

In order to demonstrate entanglement we use the Peres-Horodecki criterion [20] stating that separable two-qubit states have a positive partial transpose (PPT). Considering the observable $\hat{W}$, we first compute its maximum expectation value w_{ppt} (see Supplemental Material Sec. II [21]) for separable two-qubit states ρ_{qubit}, i.e., $\rho_{\mathrm{qubit}} \geq 0$ and $\mathrm{tr}(\rho_{\mathrm{qubit}}) = 1$:

$$\begin{aligned} w_{\mathrm{ppt}} = \max_{\rho_{\mathrm{qubit}}} & \mathrm{tr}(\rho_{\mathrm{qubit}}\hat{W}) \\ \text{s.t. } & (i)\, \rho_{\mathrm{qubit}}^{T_1} \geq 0, \\ & (ii)\, \rho_{i,i} = P_{ii}, \end{aligned} \tag{5}$$

where $\rho_{i,i}$ denote the diagonal elements of ρ_{qubit}. The advantage of using this witness together with condition (ii) rather than a fixed linear combination of observables as done in Ref. [13] is that we use all our knowledge of the diagonal elements of the density matrix. This is equivalent to considering a witness constructed from all possible linear combinations of $\sigma_{\alpha_1}^{(1)} \otimes \sigma_{\alpha_2}^{(2)}$, $\sigma_0^{(1)} \otimes \sigma_0^{(2)}$, $\sigma_0^{(1)} \otimes \mathbb{1}$ and $\mathbb{1} \otimes \sigma_0^{(2)}$ which can detect more entangled states. If we restrict ourselves to qubit states, the quantities P_{ij} are given by the measured quantities $P_{\mathrm{nc,nc}}$, $P_{\mathrm{nc,c}}$, $P_{\mathrm{c,nc}}$ and $P_{\mathrm{c,c}}$ without displacement fields where, for example, $P_{\mathrm{nc,c}}$ is the joint probability of having a "no-click" event on the detector on mode 1 and a "click" event on mode 2. If the measured value of $\langle\hat{W}\rangle$ is larger than w_{ppt}, we can conclude that our state is entangled.

To elaborate on the robustness of our witness, let us consider the state $\rho_\eta = (1-\eta)|00\rangle\langle 00|_{AB} + \eta|\psi\rangle\langle\psi|_{AB}$ which corresponds to adding losses on the state $|\psi\rangle_{AB}$. One can easily check that there always exist settings α_1 and α_2 such that $\mathrm{tr}(\rho_\eta\hat{W}) > w_{\mathrm{ppt}}$ for all efficiencies η different than 0 (see Supplemental Material Sec. II [21]). This means that $\hat{W}$ has the ability to detect entanglement for arbitrary loss on the state. Note the fact that we considered detectors with unit efficiencies is still a valid description of

our measurement apparatus since one can transfer the inefficiency of the detector to loss on the state (see Supplemental Material Sec. IV [21]).

In practice, the amplitude of displacement operations may vary from run to run which could lead to false witness violations. To take into account those fluctuations, we first bound them experimentally and then maximize w_{ppt} accordingly, which leads to $\tilde{w}_{\mathrm{ppt}} \geq w_{\mathrm{ppt}}$ (see Supplemental Material Sec. III [21]). Note that in order to reduce the impact of amplitude fluctuations we choose the mean amplitudes such that $\partial^2 w_{\mathrm{ppt}}/\partial\alpha_1\partial\alpha_2 = 0$, which in our case holds true for $\alpha_1 = \alpha_2 \approx 0.83$.

So far, we derived the maximum expectation value w_{ppt} a separable two-qubit state can achieve. To remove the assumption on the dimension and hence to obtain a state-independent entanglement witness, we derive a general bound for all separable states (see Supplemental Material Sec. III [21])

$$w_{\mathrm{ppt}}^{\mathrm{max}} = \tilde{w}_{\mathrm{ppt}} + p_1^* + p_2^* + 2\beta\sqrt{(p_1^* + p_2^*)(1 - p_1^* - p_2^*)}, \quad (6)$$

where $\beta = 2\alpha_1\alpha_2 e^{-(\alpha_1^2+\alpha_2^2)}\sqrt{2(\alpha_1^4+\alpha_2^4)}$ with $\alpha_i \in \mathbb{R}^+$ and p_i^* denote upper bounds on the probabilities of having more than one photon in mode i. The latter can be bounded in practice by measuring twofold coincidences after a 50/50 beam splitter. We can thus conclude about entanglement in an arbitrary state ρ if $\mathrm{tr}(\rho\hat{W}) > w_{\mathrm{ppt}}^{\mathrm{max}}$.

Experiment.—A schematic overview of the experimental implementation is presented in Fig. 2. We use two nonlinear crystals as type-II SPDC sources pumped by a pulsed laser at $\lambda_p = 771.7$ nm to create nondegenerate photons at $\lambda_s = 1541.3$ (signal) and $\lambda_i = 1546.1$ nm (idler). The photon pair creation probability per pump pulse for each crystal is kept at $P_{\mathrm{pair}} \approx 3 \times 10^{-3}$ in order to keep the probability of having double-pair emissions sufficiently low. Signal and idler modes are separated after their generation at the polarizing beam splitters (PBS) and coupled into single-mode optical fibers. The idler photons are then sent to a 50/50 beam splitter (BS) and are spectrally filtered by a dense wavelength division multiplexer (DWDM) with a 100 GHz passband (ITU channel 39). We therefore ensure high-purity heralded signal photons and achieve a spectral overlap of 99.9% between idler photons originating from the two independent sources (see Supplemental Material Sec. VIII [21]). To reduce the photon noise due to residual seed-pulse photons (see below), and unwanted optical reflections, arriving before the heralding idler photons, a gate of 2 ns is generated by an electro-optic intensity modulator (EOM) to temporally filter before the detector. The EOM has an insertion loss of 5.0 dB and an extinction ratio of 33 dB.

In order to perform the displacement-based measurement on the state shared between Alice and Bob, we generate a

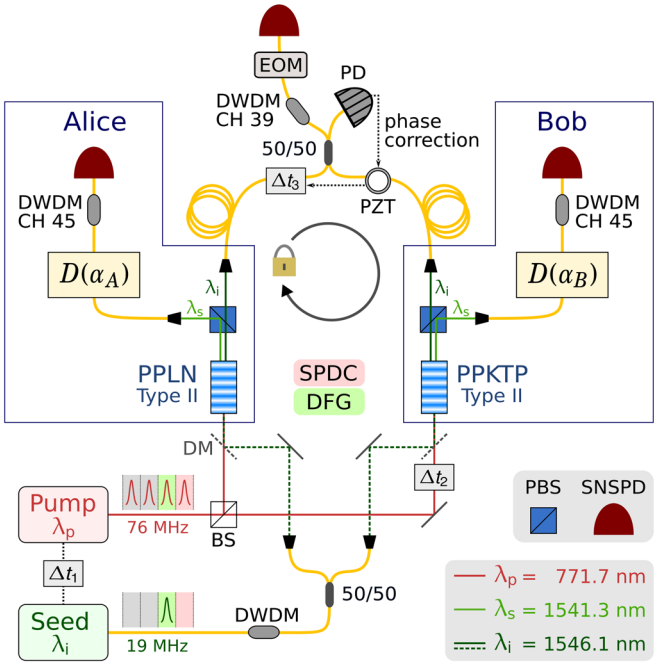

FIG. 2. Simplified schematic of the experimental setup for the heralded distribution and certification of single-photon path entanglement. A periodically poled lithium niobate (PPLN) and a periodically poled potassium titanyl phosphate (PPKTP) bulk nonlinear crystal are pumped by a pulsed Ti:sapphire laser at λ_p in the picosecond regime with a repetition rate of 76 MHz for collinear type-II SPDC and seeded by a pulsed DFB laser at λ_i with a repetition rate of 19 MHz for DFG. The idler photons are sent to the central station and herald entanglement distribution. The signal photons and coherent states are sent to Alice and Bob, respectively, in order to perform the displacement-based measurement. Photons are detected by three superconducting nanowire single-photon detectors (SNSPD).

coherent state with the same spectral, temporal, and polarization properties as the single photon signal via a difference frequency generation (DFG) process by stimulating the nonlinear crystals with a pulsed distributed feedback (DFB) seed laser at a wavelength $\lambda_i = 1546.1$ nm and repetition rate 19 MHz. The seed laser is driven from well below to above the lasing threshold each cycle to phase randomize the coherent state. For the implementation of the displacement-based measurement (see Supplemental Material Sec. VII [21]), the single-photon and the coherent states are temporally brought to coincidence in an asymmetric Mach-Zehnder interferometer (AMZI) followed by a PBS to project the single-photon and the coherent states into the same temporal and polarization modes, which realizes the displacement operation [15]. We increase the spectral overlap between single-photon and coherent states by local filtering with DWDMs (100 GHz passband at ITU channel 45).

To fulfill the phase stability requirement (see Supplemental Material Sec. VI [21]), the central interferometer is phase locked using the residual seed laser pulses at

the central station. A piezoelectric fiber stretcher (PZT) with a half-wavelength voltage of $V_\pi = 0.18$ V and an optical delay range of about 0.57 ps is actively controlled such that the seed power at the second output port of the 50/50 BS, measured with a photodiode (PD), is maximized. Note that we do not require phase-coherent pump pulses (see Supplemental Material Sec. VI [21]). Additionally, and specific to our implementation of the displacement-based measurement, the phase difference between the AMZIs is stabilized (see Supplemental Material Sec. VII [21]).

In order to demonstrate the feasibility of long-distance entanglement distribution, we extend the central interferometer arm lengths from initially $l = 42$ m to $l = 1.0$ km by inserting two fiber coils. This change additionally requires active polarization control before the 50/50 BS as well as active compensation of slow relative drifts in optical length between the two interferometer arms. Therefore, electronic polarization controllers (Phoenix Photonics PSC) are inserted after the fiber coils to minimize the seed power at the second output ports of the fiber PBSs whose first output ports are connected to the polarization maintaining 50/50 BS at the end of the central interferometer. The slow relative optical length drifts are compensated by actively setting Δt_3 (see Fig. 2) with a motorized delay line such that the voltage applied to the PZT is kept in range. In this way, we achieve long-term phase stabilization as shown in Fig. 3 for a duration of 8 h.

The photons are detected by three in-house-developed MoSi superconducting nanowire single-photon detectors (SNSPD) with efficiencies $\eta_d > 60\%$ and recovery times $\tau_{\mathrm{rec}} < 35$ ns. Time correlated single-photon counting (ID Quantique ID900) is used to register the events of a signal photon detected by Alice, by Bob, and coincidences conditioned on the detection of an idler photon at the central station within a 400 ps window with respect to the 19 MHz clock signal. In the α-basis, we monitor the displacement amplitudes by tracking the detection rates caused by coherent states arriving 1 cycle (52 ns) later than the expected signal photons.

Results.—A measurement of the witness as a function of the relative phase between Alice's and Bob's displacement operations is shown in Fig. 4. After the relative phase is set to $(\theta_B - \theta_A) = 0$, counts were acquired in the α-basis for 1 h and subsequently in the z-basis for 2.5 h by blocking the coherent state paths in the measurement interferometers. From the "click"-"no-click" events recorded by Alice and Bob, the corresponding joint probabilities are deduced (see Supplemental Material Sec. IX [21]). We separately determined the probability of having more than one photon locally in a Hanbury Brown–Twiss experiment for both Alice and Bob. Together with the joint probabilities measured in the z-basis as well as the displacement parameter amplitudes used in the α-basis measurement, we compute the estimator (see Supplemental Material Sec. V [21]) for the maximal separable bound $w_{\mathrm{ppt}}^{\max}$ according to Eq. (6). The experimental value for the expectation value $w_\rho^{\exp}$ of the witness $\hat{W}$ is computed from the measured joint probabilities in the α-basis by

$$w_\rho^{\exp} = (P_{\mathrm{nc,nc}} + P_{\mathrm{c,c}} - P_{c,\mathrm{nc}} - P_{\mathrm{nc,c}})|_{\alpha_1,\alpha_2}. \qquad (7)$$

For the analysis of uncertainties on the separable bound $\sigma_{\mathrm{ppt}}^{\max}$ and on the experimental value of the witness $\sigma_\rho^{\exp}$ we assume the coincidence probabilities to be independent and identically distributed (i.i.d.) random variables (see Supplemental Material Sec. V [21]). The obtained results, as shown in Table I, certify a violation of the entanglement witness by more than 5 standard deviations at a heralding rate of at least 1.4 kHz for fiber distances of $l = 42$ m and

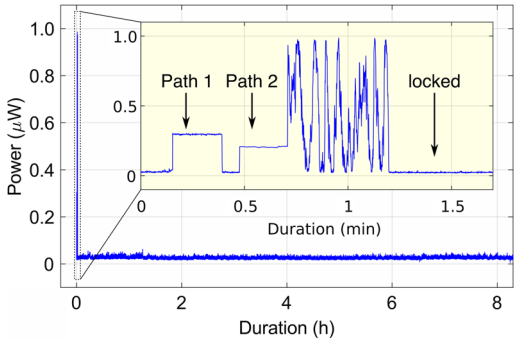

FIG. 3. Characterization measurement of the central interferometer phase locking for $l = 1.0$ km. The graph shows the measured seed power at the 50/50 BS output port 1 over a duration of 8 h. The active feedback on the piezoelectric fiber stretcher and the time delay feedback are turned on after 1.2 min (inset). During the initial 1.2 min, first path 1 of the interferometer is left open only, then path 2, and afterwards both paths are opened leading to interference.

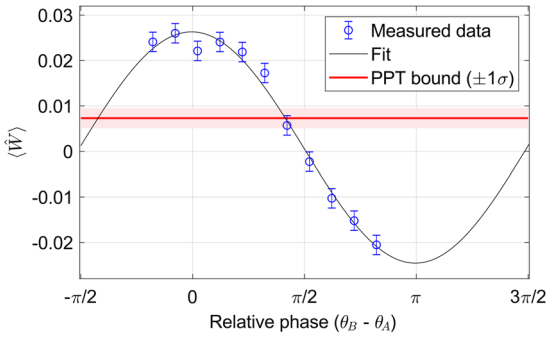

FIG. 4. Expectation value and PPT bound $w_{\mathrm{ppt}}^{\max}$ of the entanglement witness as a function of the relative phase $(\theta_B - \theta_A)$ between the displacement measurements for Alice and Bob with $l = 1.0$ km. Values of $\langle \hat{W} \rangle$ larger than $w_{\mathrm{ppt}}^{\max}$ demonstrate entanglement. For each phase setting, counts were acquired for 200 s in the α-basis with $\alpha_1 = 0.818^{+0.004}_{-0.003}$ and $\alpha_2 = 0.830^{+0.006}_{-0.007}$ indicating the mean, maximum, and minimum displacement amplitudes. Error bars of the measured data represent 1 standard deviation.

TABLE I. Measured value w_ρ^{exp} and calculated separable bound $w_{\mathrm{ppt}}^{\mathrm{max}}$ of the entanglement witness for fibers of length l inserted in each arm of the central interferometer at an observed heralding rate ν_h and signal-to-noise ratio (SNR). The witness is violated by $k = (w_\rho^{\mathrm{exp}} - w_{\mathrm{ppt}}^{\mathrm{max}})/(\sigma_{\mathrm{ppt}}^{\mathrm{max}} + \sigma_\rho^{\mathrm{exp}})$ standard deviations.

l	ν_h (kHz)	SNR	w_ρ^{exp}	$w_{\mathrm{ppt}}^{\mathrm{max}}$	k
42 m	1.4	12	0.0206(8)	0.0071(16)	5.6
1.0 km	1.6	5	0.0253(7)	0.0071(22)	6.2

$l = 1.0$ km inserted in each arm of the central interferometer. The higher total heralding rate in the case of $l = 1.0$ km is due to an elevated noise contribution. The larger statistical significance of the result with $l = 1.0$ km compared to $l = 42$ m is mainly attributed to a different alignment setting in the measurement AMZIs leading to an increase of the transmission on the entangled state (see Supplemental Material Sec. IX [21]).

Discussion.—Single-photon quantum repeater schemes are promising for fiber-based long-distance entanglement distribution because of their favorable transmission loss scaling, their robustness to memory and detector inefficiencies and the need for fewer resources than protocols based on two-photon detections [5]. We demonstrated the feasibility of such a scheme by actively stabilizing the phase of an interferometer with arm lengths of 1.0 km and utilizing local displacement-based measurements for entanglement certification. In our scheme the phase difference between the AMZIs also needs to be stabilized (see Supplemental Material Sec. VII [21]), however, in a quantum repeater these AMZIs could be replaced, and the displacement performed, by quantum memories [25,26].

In principle, the scheme can be extended for real world applications by using two individual pump lasers, adding fiber before the sources to distribute the seed pulses and further increasing the size of the central interferometer. The main technical challenge in such an implementation is the increase of phase noise in a larger central interferometer [27]. This would not only degrade the entanglement, but also increase the leakage of residual seed laser pulse photons towards the heralding detector. Our solution to suppress them with an EOM introduces unwanted loss on the heralding photons, however, a better solution would be to develop a gated SNSPD for the central station.

In conclusion, we demonstrated the heralded distribution of single-photon path entanglement in a repeater-like architecture. For a fiber distance of 2×1.0 km inserted in the central interferometer we achieve a heralding rate of 1.6 kHz and we certify a violation of the entanglement witness by 6.2 standard deviations. These results highlight the feasibility and challenges associated with realizing DLCZ-like quantum repeater architectures.

The authors would like to thank C. Autebert, J.-D. Bancal, F. Bussières, C. Barreiro, A. Boaron, and P. Remy for useful discussions and technical support. This work was supported by the Swiss National Science Foundation SNSF (Grants No. 200021_159592, No. 200020_182664, and No. PP00P2-179109), COST (SBFI/SNF) IZCNZ0-174835, and the European Union's Horizon 2020 research and innovation programme under Grant Agreement No. 820445 (Quantum Internet Alliance).

P. C. and E. V. contributed equally to this work.

*Present address: Université Côte d'Azur, CNRS, Institut de Physique de Nice, Parc Valrose, F-06108 Nice Cedex 2, France.

†Robert.Thew@unige.ch

[1] H. J. Kimble, Nature (London) **453**, 1023 (2008).
[2] S. Wehner, D. Elkouss, and R. Hanson, Science **362**, eaam9288 (2018).
[3] H.-J. Briegel, W. Dür, J. I. Cirac, and P. Zoller, Phys. Rev. Lett. **81**, 5932 (1998).
[4] S. M. Tan, D. F. Walls, and M. J. Collett, Phys. Rev. Lett. **66**, 252 (1991).
[5] N. Sangouard, C. Simon, H. de Riedmatten, and N. Gisin, Rev. Mod. Phys. **83**, 33 (2011).
[6] L.-M. Duan, M. D. Lukin, J. I. Cirac, and P. Zoller, Nature (London) **414**, 413 (2001).
[7] C. Simon, H. de Riedmatten, M. Afzelius, N. Sangouard, H. Zbinden, and N. Gisin, Phys. Rev. Lett. **98**, 190503 (2007).
[8] L. Slodička, G. Hétet, N. Röck, P. Schindler, M. Hennrich, and R. Blatt, Phys. Rev. Lett. **110**, 083603 (2013).
[9] A. Delteil, Z. Sun, W. B. Gao, E. Togan, S. Faelt, and A. Imamoglu, Nat. Phys. **12**, 218 (2016).
[10] R. Stockill, M. J. Stanley, L. Huthmacher, E. Clarke, M. Hugues, A. J. Miller, C. Matthiesen, C. Le Gall, and M. Atatüre, Phys. Rev. Lett. **119**, 010503 (2017).
[11] P. C. Humphreys, N. Kalb, J. P. J. Morits, R. N. Schouten, R. F. L. Vermeulen, D. J. Twitchen, M. Markham, and R. Hanson, Nature (London) **558**, 268 (2018).
[12] Y. Yu, F. Ma, X.-Y. Luo, B. Jing, P.-F. Sun, R.-Z. Fang, C.-W. Yang, H. Liu, M.-Y. Zheng, X.-P. Xie, W.-J. Zhang, L.-X. You, Z. Wang, T.-y. Chen, Q. Zhang, X.-H. Bao, and J.-W. Pan, Nature (London) **578**, 240 (2020).
[13] F. Monteiro, V. C. Vivoli, T. Guerreiro, A. Martin, J.-D. Bancal, H. Zbinden, R. T. Thew, and N. Sangouard, Phys. Rev. Lett. **114**, 170504 (2015).
[14] V. C. Vivoli, P. Sekatski, J.-D. Bancal, C. C. W. Lim, A. Martin, R. T. Thew, H. Zbinden, N. Gisin, and N. Sangouard, New J. Phys. **17**, 023023 (2015).
[15] M. G. Paris, Phys. Lett. A **217**, 78 (1996).
[16] K. Banaszek and K. Wódkiewicz, Phys. Rev. Lett. **82**, 2009 (1999).
[17] A. Kuzmich, I. A. Walmsley, and L. Mandel, Phys. Rev. Lett. **85**, 1349 (2000).
[18] G. Björk, P. Jonsson, and L. L. Sánchez-Soto, Phys. Rev. A **64**, 042106 (2001).
[19] B. Hessmo, P. Usachev, H. Heydari, and G. Björk, Phys. Rev. Lett. **92**, 180401 (2004).
[20] M. Horodecki, P. Horodecki, and R. Horodecki, Phys. Lett. A **223**, 1 (1996).

[21] See Supplemental Material at http://link.aps.org/supplemental/10.1103/PhysRevLett.125.110506 for theoretical calculations, details on the experimental implementation and additional data to support the results, which includes Refs. [22–24].
[22] A. R. McMillan, L. Labonté, A. S. Clark, B. Bell, O. Alibart, A. Martin, W. J. Wadsworth, S. Tanzilli, and J. G. Rarity, Sci. Rep. **3**, 2032 (2013).
[23] P. J. Mosley, Generation of heralded single photons in pure quantum states, Ph.D. Thesis, University of Oxford, 2007.
[24] N. Bruno, A. Martin, and R. Thew, Opt. Commun. **327**, 17 (2014).
[25] P. Jobez, Stockage multimode au niveau quantique pendant une milliseconde, Ph. D. thesis, Université de Genève, 2015.
[26] K. Kutluer, E. Distante, B. Casabone, S. Duranti, M. Mazzera, and H. de Riedmatten, Phys. Rev. Lett. **123**, 030501 (2019).
[27] J. Minář, H. de Riedmatten, C. Simon, H. Zbinden, and N. Gisin, Phys. Rev. A **77**, 052325 (2008).